

Bulk viscosity model for near-equilibrium acoustic wave attenuation

Jeffrey Lin,^{1, a)} Carlo Scalo,² and Lambertus Hesselink¹

¹⁾*Department of Electrical Engineering, Stanford University, Stanford, CA, 94305 USA*

²⁾*School of Mechanical Engineering, Purdue University, West Lafayette, IN, 47907 USA*

(Dated: February 20, 2022)

Acoustic wave attenuation due to vibrational and rotational molecular relaxation, under simplifying assumptions of near-thermodynamic equilibrium and absence of molecular dissociations, can be accounted for by specifying a bulk viscosity coefficient μ_B . In this paper, we propose a simple frequency-dependent bulk viscosity model which, under such assumptions, accurately captures wave attenuation rates from infrasonic to ultrasonic frequencies in Navier–Stokes and lattice Boltzmann simulations. The proposed model can be extended to any gas mixture for which molecular relaxation timescales and attenuation measurements are available. The performance of the model is assessed for air by varying the base temperature, pressure, relative humidity h_r , and acoustic frequency. Since the vibrational relaxation timescales of oxygen and nitrogen are a function of humidity, for certain frequencies an intermediate value of h_r can be found which maximizes μ_B . The contribution to bulk viscosity due to rotational relaxation is verified to be a function of temperature, confirming recent findings in the literature. While μ_B decreases with higher frequencies, its effects on wave attenuation become more significant, as shown via a dimensionless analysis. The proposed bulk viscosity model is designed for frequency-domain linear acoustic formulations but is also extensible to time-domain simulations of narrow-band frequency content flows.

PACS numbers: PACS: 43.28.Bj, 43.28.Js, 43.35.Ae, 43.35.Fj

I. INTRODUCTION

The viscous stress tensor of an isotropic Newtonian fluid reads

$$\sigma_{ij} = -p\delta_{ij} + \tau_{ij} = \left(-p + \mu' \frac{\partial u_k}{\partial x_k}\right) \delta_{ij} + 2\mu S_{ij}, \quad (1)$$

where p is the thermodynamic pressure, u_i and x_i are the velocity component and spatial coordinate along the i -th direction, $S_{ij} = 1/2(\partial u_i/\partial x_j + \partial u_j/\partial x_i)$ is the strain-rate tensor, and μ' is the second coefficient of viscosity

$$\mu' = \mu_B - \frac{2}{3}\mu, \quad (2)$$

where μ_B and μ are the bulk (or volume) and shear (or dynamic) viscosity, respectively. While shear viscosity is a well-characterized fluid property, bulk viscosity is neglected in most fluid problems due to its often unknown value. The commonly adopted Stokes' hypothesis, which holds for dilute, monatomic gases, in fact reads $\mu' = -\frac{2}{3}\mu$, implying $\mu_B = 0$. However, for many fluids and flows of interest, μ_B cannot be neglected.¹ Furthermore, in the context of wave attenuation modeling, bulk viscosity is not interpreted as a pure fluid property, as it depends on flow conditions, e.g., acoustic frequency.

Experimental and semi-empirical characterizations of wave attenuation in air confirm that bulk viscosity effects are due to molecular relaxation, a non-equilibrium thermodynamic process which is sufficiently important

so as to affect acoustic energy but not so intense as to require a full description of molecular-level energy exchange dynamics.^{2–7} Bulk viscosity can significantly affect the attenuation rate of freely propagating waves in mixtures composed of multi-atomic species—for example, $\mu_B \simeq 2000\mu$ for CO_2 ^{1,8} or for dry air at 110 Hz—and its effect accumulates over each cycle of acoustic wave propagation, making it very important at higher (e.g., ultrasonic) acoustic frequencies. The accurate knowledge of bulk viscosity values is desired in high-fidelity simulations of aeroacoustics problems, with applications including thermoacoustic energy conversion and imaging, acoustic energy transfer (AET)⁹, ultrasonic air-coupled non-destructive examination, and supersonic flow.¹⁰ In other applications, such as for acoustic trapping, the accurate prediction of heat generation due to both shear and bulk viscosity specifically is critical.¹¹ Bulk viscosity effects are also very important in the presence of strong spatial density gradients, such as in shock waves, which yield high (negative) values of the velocity divergence term in Eq. (1). The distinction between losses due to shear or bulk viscosity effects is also relevant to acoustic problems in which the phasing of dilatation can be decoupled from that of pressure.

Numerical simulations of wave attenuation due to bulk viscosity effects and estimates of bulk viscosity coefficient values have been attempted at various scales of fidelity by previous authors. Eu and Ohr¹² have shown that Navier–Stokes simulations without bulk viscosity fail to fully capture absorption and dispersion for polyatomic gases, and Claycomb et al.^{13,14} have shown that under rarefied flow conditions and Mach numbers up to 15, the introduction of bulk viscosity can improve predictions of shock thickness and separation in a double cone geometry. Wagnild et al.¹⁵ evaluated vibrational relaxation

^{a)}Electronic mail: linjef@stanford.edu; Corresponding author.

effects in hypersonic boundary layers using direct numerical simulations, and Valentini et al.¹⁶ used direct molecular simulation to predict rotational and vibrational relaxation effects in high-temperature nitrogen. Salomons et al.¹⁷ performed lattice Boltzmann method (LBM) simulations without accounting for bulk viscosity effects, finding that the accuracy of simulated acoustic wave attenuation is limited by LBM stability and dissipation to short propagation distances, low frequencies, and high viscosity. Viggen¹⁸ developed a LBM approach which captures absorption and dispersion due to both shear and bulk viscosity for a hypothetical single-species fluid, with results in agreement with theoretical predictions. Ern and Giovangigli^{19–21} developed multicomponent transport algorithms to accurately calculate various transport coefficients, including bulk viscosity associated with rotational molecular relaxation.

To the authors' knowledge, established methods providing the value of μ_B for the prediction of acoustic wave attenuation rates are currently missing in the literature. In this manuscript, we present a model for μ_B valid in near-equilibrium acoustic energy absorption conditions, which can be adopted in frequency-domain formulations as well as narrow-band time-domain simulations.

A. Bulk viscosity origins and measurements

While bulk viscosity is negligible for dilute monatomic gases, as confirmed theoretically and experimentally,¹ it is generally non-zero for polyatomic gases. For example, a diatomic molecule has six degrees of freedom: three translational, two rotational, and one vibrational. The translational degrees of freedom relax to equilibrium conditions relatively quickly, while the rotational and vibrational degrees of freedom have longer relaxation times, hence delaying thermodynamic equilibrium when excited. At thermodynamic equilibrium, the average energy for each translational and rotational degree of freedom is $k_B T/2$, where k_B is Boltzmann's constant and the fluid temperature T is equal to the apparent translational temperature T_{tr} and rotational temperature T_{rot} . The corresponding translational and rotational energies are given by

$$E_{tr} = \frac{3}{2} R_{gas} T_{tr} \quad (3)$$

$$E_{rot} = \frac{1}{2} \frac{5 - 3\gamma}{\gamma - 1} R_{gas} T_{rot}, \quad (4)$$

where R_{gas} is the specific gas constant and γ is the ratio of specific heats. The vibrational energy associated with the k -th molecular species is derived from the Boltzmann distribution and is given by

$$E_{vib,k} = \frac{n_k}{n} R_{gas} T_{vib,k}^* \exp\left(-\frac{T_{vib,k}^*}{T_{vib,k}}\right), \quad (5)$$

where n_k/n is the species mole fraction, and $T_{vib,k}^*$ and $T_{vib,k}$ are, respectively, the characteristic molecular vibration temperature and species vibrational temperature. At thermodynamic equilibrium, the fluid temperature T is also equal to the apparent vibrational temperatures $T_{vib,k}$, and there is zero net energy exchange among the degrees of freedom.

However, under thermodynamic non-equilibrium conditions, both vibrational and rotational energies diverge from their equilibrium values, and the process of relaxation to equilibrium conditions is represented by the bulk viscosity coefficient. The equivalent relaxation process for translational degrees of freedom is embedded within the shear viscosity coefficient. Such attenuative processes are of particular interest in sound propagation, where pressure and velocity fluctuations (i.e. fluctuations in translational molecular energy) establish a cycle of compressions and expansions accompanied by temperature fluctuations. However, unlike shear viscosity, absorption of sound is the primary effect of bulk viscosity, and the experimental characterization of bulk viscosity in various materials has predominantly been completed through various forms of acoustic wave attenuation measurements.^{22–25}

Bulk viscosity, μ_B , as defined in the present paper by Eqs. (1) and (2), is sometimes referred to in the literature as volume viscosity²⁶, dilatational viscosity²⁷, expansion viscosity^{28,29}, or the second coefficient of viscosity³⁰. The second coefficient of viscosity μ' , as defined in the present paper by Eq. (2),³¹ has also been referred to by some authors^{28,29} as the bulk viscosity; this definition results in a (misleadingly) negative value for bulk viscosity in dilute, monatomic gases. According to the convention adopted in the present paper, bulk viscosity is $\mu_B = 0$ for dilute monatomic gases, consistent with literature in acoustics and molecular kinetics.²⁵

The physical complexity of the relaxation processes modeled by bulk viscosity contribute further to the confusion in the literature. Some authors⁴ attribute bulk viscosity to rotational molecular relaxation only, while others⁸ also include vibrational effects. In the present manuscript, both the effects of vibrational and rotational molecular relaxation are incorporated within μ_B by definition.

In acoustics, bulk viscosity effects due to rotational relaxation are of secondary importance; for air $\mu_{B,rot} \approx 0.6\mu$ for approximately all frequencies, with some dependency on temperature,⁴ as discussed later. On the other hand, the vibrational relaxation contribution can be relatively large, e.g., $\mu_{B,vib} \approx 25\mu$ at 1000 Hz in dry air under standard atmospheric conditions.

The combined effect of rotational and vibrational relaxation can be inferred from the absorption coefficient, α —a measure of the relative wave amplitude attenuation per propagation distance—which is of particular interest in atmospheric acoustics. For a purely traveling tonal disturbance, spatial attenuation follows the exponential

law

$$P_{amp} = P_{amp,0} e^{\alpha\lambda[-(x-x_0)/\lambda]} \quad (6a)$$

$$= P_{amp,0} e^{\alpha\lambda[-(t-t_0)\omega/2\pi]}, \quad (6b)$$

where $P_{amp,0}$ is the amplitude of the traveling wave at position $x = x_0$ or, equivalently, at time $t = t_0$, and ω is the angular frequency and λ is the wavelength.

The classical acoustic absorption coefficient, or the Stokes-Kirchoff attenuation coefficient, only accounts for thermoviscous attenuation,³²

$$\alpha_{sk} = \frac{\omega^2}{2\rho_0 a_0^3} \left[\frac{4}{3}\mu + \frac{(\gamma-1)^2 \kappa}{\gamma R_{gas}} \right], \quad (7)$$

where ρ_0 and a_0 are the base density and speed of sound, and κ is the thermal conductivity. The first term on the right-hand side of Eq. (7) represents the effect of viscous dissipation and the second term represents the effect of heat conduction; both processes have characteristic timescales in the gigahertz range for gases such as argon, helium, and neon.³² As a result, the rate of lossy, thermoviscous momentum transfer is small, compared to momentum transfer due to ideal wave propagation. The classical absorption coefficient is derived from simplifying the more general form of the complex thermoviscous wave number of a damped monochromatic traveling wave,

$$\alpha_{sk} = \text{Im} \left[\frac{\omega}{a_0} \sqrt{\frac{(1 + i\gamma\tau_\kappa\omega)(1 + i\tau_\nu\omega)}{(1 + i\tau_\kappa\omega)}} \right] \quad (8a)$$

$$\simeq \frac{\tau_\nu\omega^2}{2a_0} + \frac{(\gamma-1)\tau_\kappa\omega^2}{2a_0} \quad (8b)$$

where $\tau_\nu = 4\mu/3\rho_0 a_0^2$ is the viscous relaxation time, $\tau_\kappa = \kappa/c_{p0}\rho_0 a_0^2$ is the conduction relaxation time where c_{p0} is the isobaric heat capacity, and the approximation is taken by neglecting higher-order terms in the quantities $\tau_\nu\omega$ and $\tau_\kappa\omega$. We note that τ_κ here should not be confused with τ_k , which is the vibrational molecular relaxation time explained in section II.

Bulk viscosity effects are attributed to the difference between the observed attenuation rate and the rate predicted by Eq. (7). The total attenuation rate therefore includes contributions from rotational and vibrational molecular relaxation effects:

$$\alpha = \alpha_{sk} + \alpha_{rot} + \sum_k \alpha_{vib}^{(k)}, \quad (9)$$

where the superscript k indicates the contribution from the k -th species. For air, the species in Eq. (9) are diatomic nitrogen ($k = \text{N}_2$) and oxygen ($k = \text{O}_2$). Other species such as water vapor do not contribute directly to Eq. (9), but instead act to adjust the vibrational relaxation frequencies.

Combining the rotational and vibrational relaxation effects into one bulk viscosity coefficient μ_B yields the

complete attenuation relation

$$\alpha = \frac{\omega^2}{2\rho_0 a_0^3} \left[\frac{4}{3}\mu + \frac{(\gamma-1)^2 \kappa}{\gamma R_{gas}} + \mu_B \right], \quad (10)$$

which is at the core of the proposed method to estimate the value of μ_B .

B. Paper Outline

The remainder of the paper is organized as follows: Section II presents the derivation of the proposed bulk viscosity model; Section III presents results from Navier-Stokes and LBM computations reproducing acoustic attenuation rates using the proposed bulk viscosity model; Section IV presents a discussion of the bulk viscosity coefficient as a function of pressure, temperature, frequency, and humidity and its non-dimensionalization; and finally, Section V discusses the limitations of the current approach and presents concluding thoughts. Appendix A 1 and Appendix A 2, respectively, provide details on the Navier-Stokes and LBM implementations used.

II. PROPOSED BULK VISCOSITY MODEL

The attenuation contributions from rotational and vibrational molecular relaxation are collapsed into one bulk viscosity coefficient, such that

$$\mu_B = \mu_B(p_0, T_0, f, h_r) \quad (11a)$$

$$= \mu_{B,rot} + \sum_k \mu_{B,vib}^{(k)}, \quad (11b)$$

where $\mu_{B,rot}$ is a function of only temperature T_0 ,⁴ and $\mu_{B,vib}$ is a function of temperature, base pressure p_0 , frequency f , and relative humidity h_r , hence yielding the general functional form of Eq. (11a). This form of μ_B is sometimes referred to in the literature³³ as frequency-dependent bulk viscosity, as absorption of acoustic energy associated with a given frequency is the primary technique for experimentally measuring the bulk viscosity in a gas. Such experimental measurements are in conditions of near-equilibrium, consistent with the assumptions made in the proposed model. In the following sections, the vibrational and rotational relaxation contributions are discussed separately.

A. Vibrational bulk viscosity

Based on the dispersion relation for plane traveling waves⁴ and statistical thermodynamics for the vibrational energy states, the attenuation contribution due to

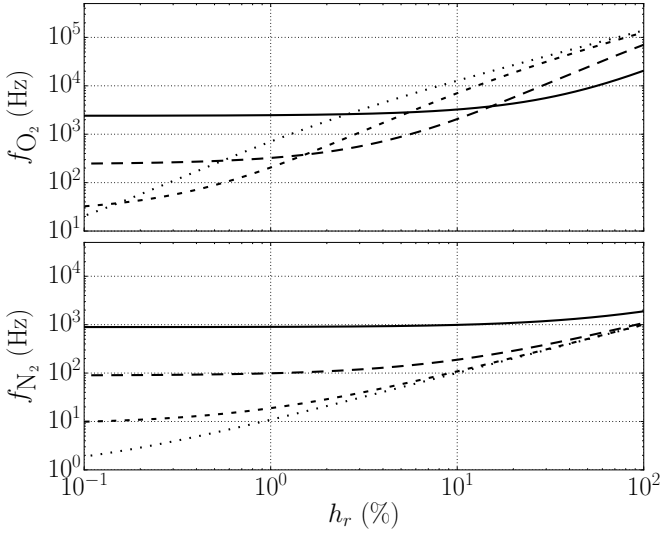


Figure 1. Vibrational molecular relaxation frequencies for oxygen $f_{O_2} = (2\pi\tau_{O_2})^{-1}$ and for nitrogen $f_{N_2} = (2\pi\tau_{N_2})^{-1}$ at $T_0 = 300$ K, plotted against relative humidity h_r , for pressures $p_0 = 0.1$ atm ($\cdot \cdot$), 1.0 atm ($--$), 10.0 atm ($-\cdot -$), and 100.0 atm ($-$).

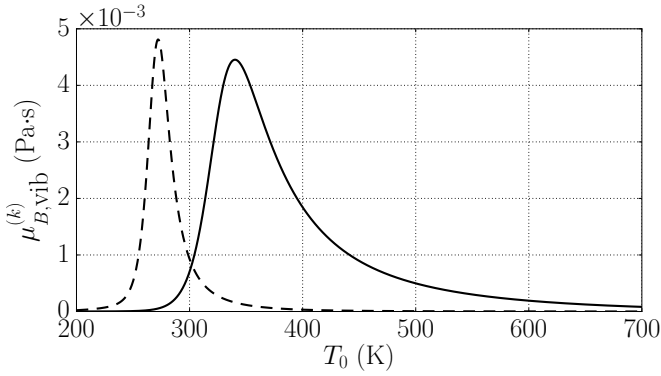


Figure 2. Modeled vibrational bulk viscosity $\mu_{B,vib}^{(k)}$ for diatomic nitrogen $k = N_2$ ($-$), and oxygen $k = O_2$ ($---$), plotted against temperature T_0 (Eq. (16)). Results presented are for $\omega/2\pi = 1$ kHz in air at $h_r = 20.0\%$ and $p_0 = 1$ atm.

vibrational molecular relaxation for the k -th species is:

$$\alpha_{vib}^{(k)} = \frac{(\gamma - 1)}{2a_0/\omega} \frac{c_{v,k}}{c_p} \frac{\omega\tau_k}{1 + (\omega\tau_k)^2} \quad (12)$$

$$c_{v,k} = \frac{n_k}{n} R_{gas} \left(\frac{T_{vib,k}^*}{T_{vib,k}} \right)^2 \exp(-T_{vib,k}^*/T_{vib,k}), \quad (13)$$

where τ_k is the vibrational molecular relaxation time, assigned according to the relaxation frequencies $f_k = (2\pi\tau_k)^{-1}$ and given for air by the semi-empirical relationships Eqs. (14a) and (14b), and c_p is the isobaric specific heat capacity. Assuming quasi-equilibrium, $T_{vib,k}$ is set equal to the base temperature T_0 .

For air, the species involved are that of oxygen ($k = O_2$) and nitrogen ($k = N_2$), with relevant parameters

$k =$	O_2	N_2
n_k/n	0.21	0.78
$T_{vib,k}^*$	2239.1 K	3352.0 K
$\tau_k(h_r = 0)$	$6.632 \cdot 10^{-3}$ s	$1.789 \cdot 10^{-2}$ s
$\tau_k(h_r = 20.0\%)$	$8.559 \cdot 10^{-6}$ s	$7.644 \cdot 10^{-4}$ s

Table I. Input parameters for air and example τ_k for Eqs. (12) and (13). τ_k are calculated for $p_0 = 1$ atm and $T_0 = 300$ K.

provided in table I. The relaxation frequencies (in Hz) of species in air are as derived by Bass et al.⁶:

$$f_{O_2} = (2\pi\tau_{O_2})^{-1} = \frac{p_0}{p_{atm}} \left(24 + 4.04 \cdot 10^4 h \frac{0.02 + h}{0.391 + h} \right) \quad (14a)$$

$$f_{N_2} = (2\pi\tau_{N_2})^{-1} = \frac{p_0}{p_{atm}} \left(\frac{T_{atm}}{T_0} \right)^{1/2} \left(9 + 280h \cdot \exp \left\{ -4.17 \left[\left(\frac{T_{atm}}{T_0} \right)^{1/3} - 1 \right] \right\} \right) \quad (14b)$$

$$\log_{10}(p_{sat}/p_{atm}) = -6.8346 (T_{3p}/T_0)^{1.261} + 4.6151, \quad (14c)$$

where $p_{atm} = 101325$ Pa is the reference atmospheric pressure; $T_{atm} = 293.15$ K, the reference atmospheric temperature; p_{sat} , the calculated saturation vapor pressure; and $T_{3p} = 273.16$ K, the triple-point isotherm temperature. The contribution of water vapor to the relaxation frequency of each species in air is determined via the relative humidity h_r , which is related to the absolute humidity h as

$$h = h_r \frac{p_{sat}}{p_0}. \quad (15)$$

Numerical constants in Eqs. (14a) and (14b) are dimensional.

Sample curves for f_{O_2} and f_{N_2} plotted against relative humidity are shown in Fig. 1. While the above relations provided above are valid for air, the vibrational bulk viscosity for a different mixture can be calculated provided species-specific characteristic molecular vibration temperatures $T_{vib,k}^*$ and relaxation frequencies f_k are known.

Combining Eqs. (9), (11b), (12) and (14), the total

vibrational bulk viscosity coefficient can be written as

$$\begin{aligned}\mu_{B,\text{vib}} &= \sum_k \mu_{B,\text{vib}}^{(k)} \\ \mu_{B,\text{vib}}^{(k)} &= \left(\frac{2\rho_0 a_0^3}{\omega^2} \right) \alpha_{\text{vib}}^{(k)} \\ &= \left[\frac{p_0}{2\pi} (\gamma - 1)^2 \left(\frac{n_k}{n} \left(\frac{T_{\text{vib},k}^*}{T_0} \right)^2 \right. \right. \\ &\quad \left. \left. \exp(-T_{\text{vib},k}^*/T_0) \right) \right] \frac{f_k}{f_k^2 + f^2}.\end{aligned}\quad (16)$$

For dry air at standard ambient temperature and pressure at 1000 Hz, $\mu_{B,\text{vib}} \simeq 22\mu$, and an example of the dependence of Eq. (16) on temperature is shown in Fig. 2 for air with $h_r = 20\%$ under standard ambient pressure.

B. Rotational bulk viscosity

The rotational molecular relaxation contribution to the overall attenuation rate, as per Eqs. (9), (10) and (11b), is

$$\alpha_{\text{rot}} = \frac{\omega^2}{2\rho_0 a_0^3} \mu_{B,\text{rot}} \quad (17)$$

where $\mu_{B,\text{rot}}$ is the rotational bulk viscosity.

Under the ideal gas assumption, the contribution to bulk viscosity from rotational relaxation is expected to only be a function of the equilibrium temperature T_0 .^{4,8} In early literature,^{4,5,34} the rotational bulk viscosity for air is described as being between $\mu_{B,\text{rot}}/\mu = 0.60 - 0.62$, where the ratio is independent of temperature. However, more recent studies³³ suggest that the ratio $\mu_{B,\text{rot}}/\mu$ should increase with temperature. Ern and Giovangigli¹⁹ calculated the rotational bulk viscosity via a linear systems approach by using expansion functions of the energy levels of each species and approximations for collision integrals, finding that the above ratio does in fact increase with temperature, as shown in Fig. 3.

It follows from Bass et al.^{6,7} that the semi-empirical expression for the combined attenuation from viscous, heat conduction, and rotational bulk viscosity effects (in air) is

$$\alpha_{\text{sk}} + \alpha_{\text{rot}} = \sqrt{\frac{T_0}{T_{\text{atm}}}} \frac{p_{\text{atm}}}{p_0} c_1 f^2, \quad (18)$$

where $c_1 = 1.84 \cdot 10^{-11} \text{ s}^2/\text{m}$.

Combining Eqs. (9), (10), (17) and (18) yields the final expression for rotational bulk viscosity used in this paper:

$$\mu_{B,\text{rot}} = \frac{\gamma p_{\text{atm}}}{2\pi^2} \sqrt{\frac{\gamma R_{\text{gas}}}{T_{\text{atm}}}} c_1 T_0 - \frac{4}{3} \mu - \frac{(\gamma - 1)^2 \kappa}{\gamma R_{\text{gas}}}. \quad (19)$$

The resulting rotational bulk viscosity yields $\mu_{B,\text{rot}}/\mu$ ratios in good agreement with Ern and Giovangigli's esti-

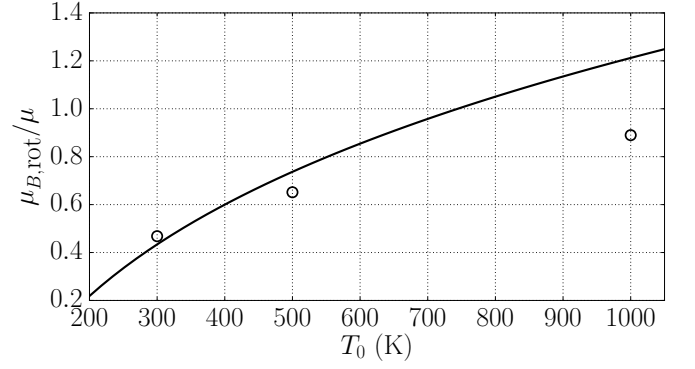


Figure 3. Ratio of the modeled rotational bulk viscosity and shear (or dynamic) viscosity, $\mu_{B,\text{rot}}/\mu$ (—), plotted against temperature (Eqs. (19) and (20)). Values for the ratio $\mu_{B,\text{rot}}/\mu$ by Ern and Giovangigli¹⁹ (○). Results presented are for air.

mates, similarly ranging from 0.433 to 1.21 between 300 K to 1000 K, as shown in Fig. 3. The shear viscosity μ used here is given by

$$\mu = \mu_{\text{ref}} (T/T_{\text{ref}})^{n_\nu} \quad (20)$$

where $n_\nu = 0.76$ is the viscosity power-law exponent and $\mu_{\text{ref}} = 1.98 \times 10^{-5} \text{ kg m}^{-1} \text{ s}^{-1}$ and $T_{\text{ref}} = 300 \text{ K}$ are the reference viscosity and temperature. Alternative formulations such as Sutherland's law³⁵ can also be used.

The overall absorption predicted using the combined effective bulk viscosity developed in the preceding Eqs. (16) and (19) is shown in Fig. 5; these curves accurately replicate experimental measurements of absorption in air.

III. TIME-DOMAIN ACOUSTIC WAVE ATTENUATION SIMULATIONS

The bulk viscosity model as developed in section II is coupled with both a Navier–Stokes and a lattice Boltzmann method (LBM) solver for verification purposes. Implementation details can be found in appendix A 1 for the Navier–Stokes solver and in appendix A 2 for the LBM solver.

The computational setup is identical for both solvers. Monochromatic planar traveling wave simulations with 4096 points per wavelength have been performed in a periodic domain. Frequencies in the range $f = 10^1 - 10^5$ Hz have been tested with relative humidity levels of dry air, 20%, and saturated air. Results for relative humidity level of 20% only are shown in Fig. 5.

A. Fully compressible Navier–Stokes simulations

In the fully compressible Navier–Stokes simulations, the governing equations for mass, momentum, and energy

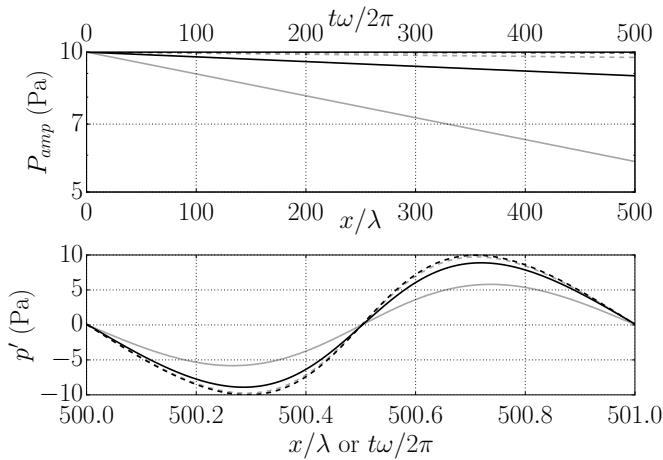


Figure 4. Time history of pressure amplitudes (top) of a freely-traveling wave for $\omega/2\pi = 1$ kHz with zero bulk viscosity (---) and with effective bulk viscosity (—), for $\omega/2\pi = 10$ kHz with zero bulk viscosity (---) and with effective bulk viscosity (—). Pressure fluctuation versus propagation distance in acoustic cycles for $x/\lambda = t\omega/2\pi > 500$ (bottom). Results presented are from the Navier–Stokes solver with conditions of $x_0 = t_0 = 0$, $h_r = 20\%$, $p_0 = 101325$ Pa, $T_0 = 300$ K, and $P_{amp,0} = 10$ Pa.

are solved in conservative form (see appendix A 1).

Due to the monochromatic nature of the wave propagation, a fixed value of the effective bulk viscosity has been used for any given frequency. Initial conditions were set as a pure isentropic traveling wave with initial pressure amplitude $P_{amp,0} = 10$ Pa. Numerical experiments yielded α as annotated in Fig. 5, which were extracted from time-series decaying pressure amplitudes, as shown in Fig. 4, where instantaneous pressure p' and amplitude P_{amp} are plotted against non-dimensional timescales as introduced in Eq. (6). Attenuation matched to within 2% for all tested combinations.

B. Lattice Boltzmann simulations

The lattice Boltzmann method is derived from Boltzmann’s kinetic theory of gases and is analogous to a finite difference method for solving the Boltzmann equation. While often used to simulate incompressible flow problems, LBM has been successfully applied to compressible flow and acoustic problems as well, and the derivation of the compressible Navier–Stokes equations from the lattice Boltzmann equations is well established.³⁶

The implementation of the proposed bulk viscosity model was carried out with a simple 2D LBM solver, using the common D2Q9 (two-dimensional, 9 velocities) scheme, with results shown in Fig. 5. The LBM solver is extended with a multiple relaxation time (MRT) model, allowing the introduction of a separate bulk viscosity parameter (see appendix A 2). The MRT model was coupled with the bulk viscosity coefficient as calculated in

section II.

The wave attenuation rate reproduced by the LBM simulations matches the semi-empirical curves with an error of under 15% for all tested combinations. Tuning of the MRT model, in particular that of the non-dimensional viscosity and the chosen diagonalization, is specific for different fluid problems, and can reduce the observed discrepancy.

IV. DISCUSSION

A. Parametric Study

In this section, we explore the functional dependency of Eq. (11a) for air only. The dependence of $\mu_{B,vib}$ and $\mu_{B,rot}$ on temperature, pressure, and frequency is shown in Fig. 7 for air with a relative humidity of $h_r = 80\%$, Fig. 8 for air with a relative humidity of $h_r = 1\%$, and Fig. 9 for dry air. The bulk viscosity is plotted as a sum of both nitrogen and oxygen species contributions.

Several trends are evident. First, the value of bulk viscosity is larger at low frequencies; while this does not necessarily mean that overall attenuation rate is larger at low frequencies, it does suggest that bulk viscosity effects cannot be completely neglected at low frequencies (e.g., infrasonic atmospheric wave propagation). Second, the bulk viscosity value increases with pressure at lower frequencies, noting the plot normalization with respect to the base pressure. Third, peaks, which at low pressures can be identified as being due to either nitrogen or oxygen vibrational frequencies, tend to merge at higher pressures, as illustrated by figures 7a and 7b.

When plotted against frequency, the vibrational bulk viscosity decreases exponentially beyond the vibrational relaxation frequency of each species, as seen in subplots (d-f) of Figs. 7 to 9. At higher frequencies, the bulk viscosity contribution from rotational relaxation defines the minimum value of μ_B .

The presence of water vapor drastically affects the magnitude of the vibrational bulk viscosity, as seen in Figs. 7 to 9. Reducing humidity from $h_r = 80\%$ to 1% increases the maximum bulk viscosity value across the considered temperature and pressure combinations, and also shifts the peak towards higher temperatures. This shift demonstrates the need to evaluate bulk viscosity as a function of humidity, temperature, as well as pressure. As a numerical example, at $T_0 = 273.15$ K, reducing humidity from 80% to 1% increases bulk viscosity for frequencies approximately below 500 Hz, but decreases bulk viscosity at mid frequency ranges (up through 20–30 kHz) and at higher frequency ranges (above 30 kHz). Increasing humidity increases the relaxation frequency of both nitrogen and oxygen species, and as seen in Eq. (16), bulk viscosity will, for each species, reach a maximum at a different combination of pressure and temperature. Because oxygen has a higher relaxation frequency than that of nitrogen, there is a region between the two frequencies

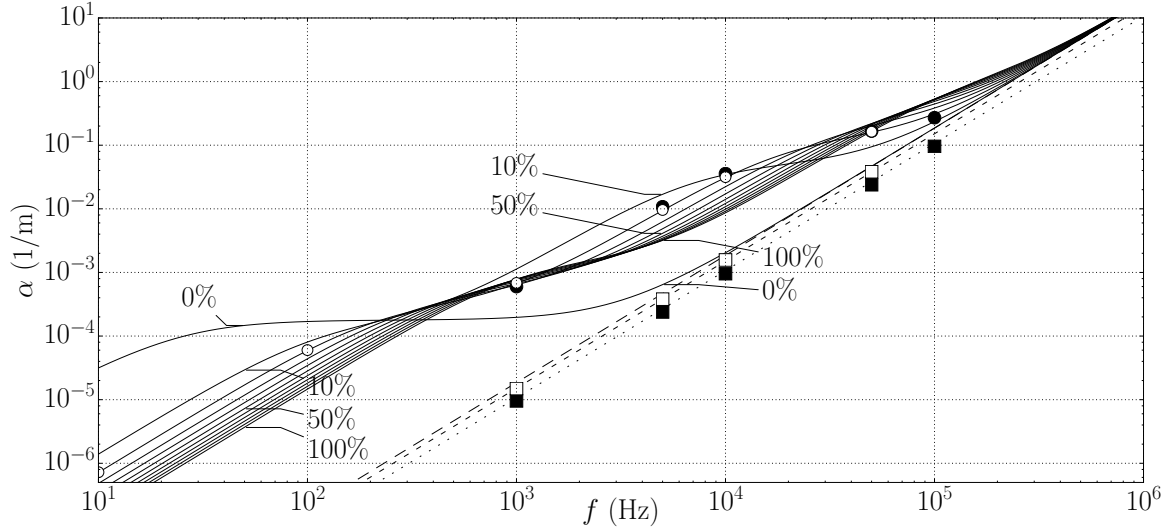


Figure 5. Acoustic amplitude attenuation rate (Eq. (6)) per unit length of propagation in air versus frequency, at $T_0 = 300$ K and $p_0 = 1$ atm, with semi-empirical expressions (—) (Eqs. (9), (16) and (19)) and Stokes-Kirchhoff attenuation expressions with rotational bulk viscosity (----), without rotational bulk viscosity (-.-.), and without bulk viscosity nor conduction (· · ·) (Eq. (7)); relative humidity in percentage reported in figure. Computationally-determined absorption via the Navier-Stokes solver for a relative humidity of $h_r = 20\%$ for zero bulk viscosity (□) and for calculated effective bulk viscosity (○); absorption in the lattice Boltzmann solver for a relative humidity of 20% for zero bulk viscosity (■) and for calculated effective bulk viscosity (●).

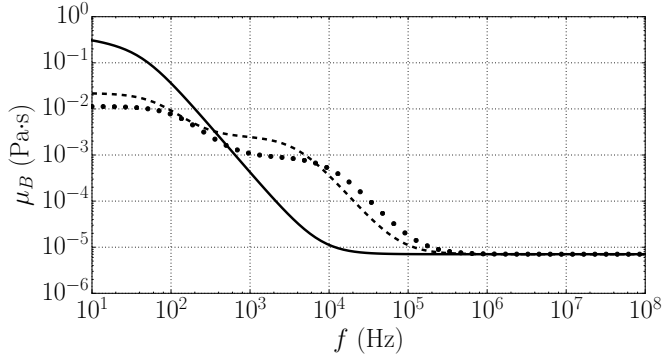


Figure 6. Bulk viscosity relative to frequency as calculated for air at $T_0 = 273.15$ K and $p_0 = 1.0$ atm for relative humidity levels of $h_r = 1\%$ (—), 40% (-.-.), and 80% (•••).

for which μ_B achieves a maximum relative to relative humidity; at lower frequencies, bulk viscosity decreases as humidity increases, and at higher frequencies, bulk viscosity increases as humidity increases, as seen in Fig. 6.

Bulk viscosity in air with zero relative humidity (Fig. 9) demonstrates no peaks with respect to temperature, as would be expected from Eqs. (14) and (16). An increase in base temperature reduces vibrational relaxation frequencies for the nitrogen species, but has no effect on the oxygen species.

B. Dimensionless scaling of bulk viscosity

1. Effective acoustic pressure

Effects related to bulk viscosity are largest near vibrational energy “peaks,” where the acoustic frequency approaches the natural frequency of a vibrational mode. In order to evaluate the effect of bulk viscosity under different conditions, we consider its effect on the acoustic effective (or mechanical) pressure. Bulk viscosity effects within the momentum and energy equations (Eq. (A1)) result in an adjustment to the thermodynamic pressure,

$$p_{\text{eff}} = p - \mu_B \nabla \cdot \vec{u}', \quad (21)$$

an expression which absorbs μ_B into the effective pressure gradient term. Per linear acoustics and assuming idealized oscillations, the continuity equation is

$$\frac{1}{\rho_0 a_0^2} \frac{\partial p'}{\partial t} + \nabla \cdot \vec{u}' = 0. \quad (22)$$

Adopting the harmonic convention $p' \sim \hat{p} e^{i\omega t}$ and assuming either standing-wave or traveling-wave phasing (both corresponding to conditions where pressure oscillations lead the velocity divergence term $\nabla \cdot \vec{u}'$ by 90°), the above equation simplifies to

$$\frac{\omega}{\rho_0 a_0^2} |\hat{p}| - \left| \widehat{\nabla \cdot \vec{u}'} \right| = 0. \quad (23)$$

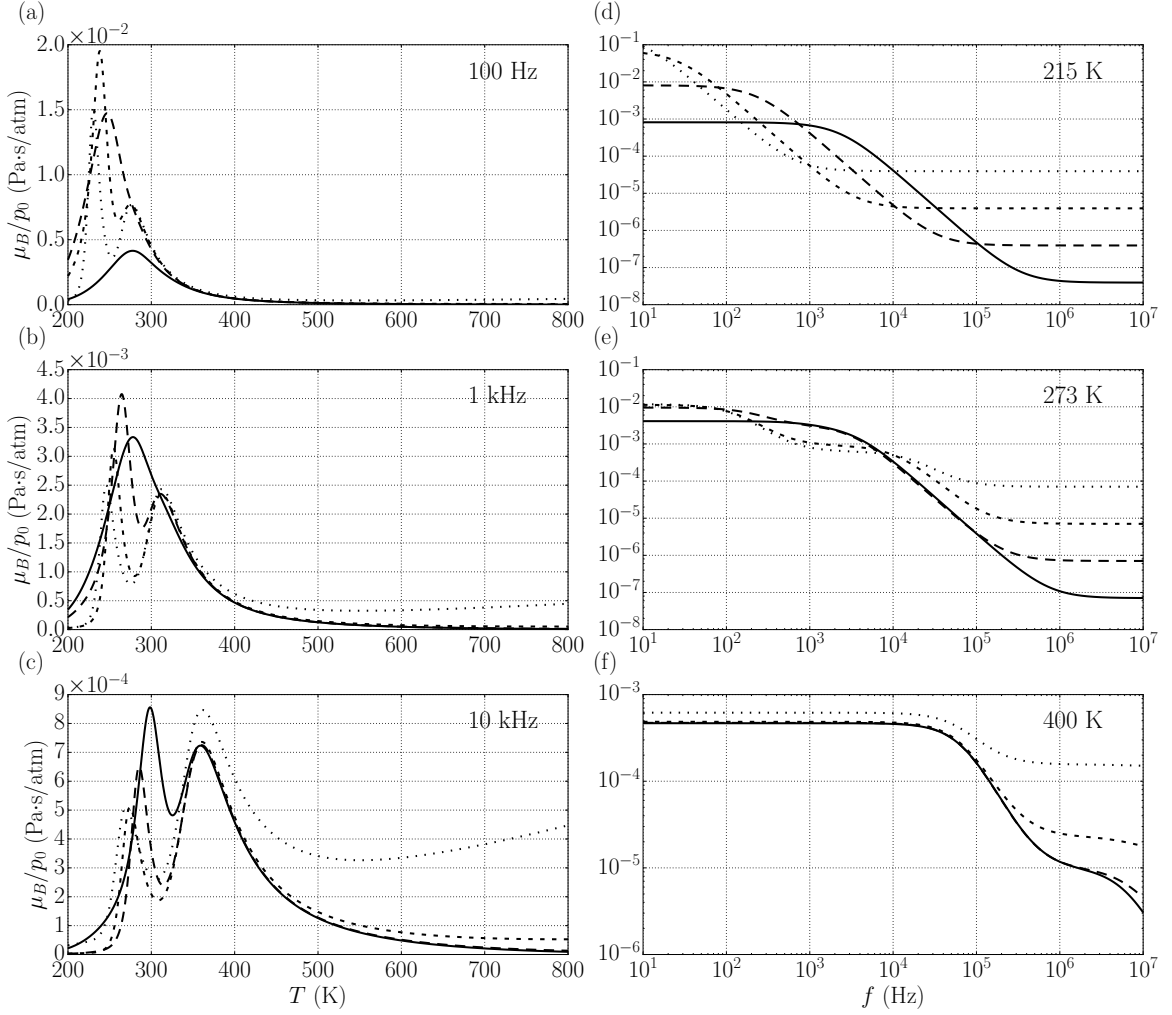


Figure 7. Pressure-normalized bulk viscosity μ_B/p_0 for air at $h_r = 80\%$. Bulk viscosity is plotted against temperature at frequencies of 100 Hz (a), 1 kHz (b), and 10 kHz (c) with pressures $p_0 = 0.1$ atm ($\cdot \cdot$), 1.0 atm ($- -$), 10.0 atm ($- \cdot -$), and 100.0 atm ($-$). Bulk viscosity is plotted against frequency at temperatures of 215.15 K (d), 273.15 K (e), and 400 K (f) with pressures $p_0 = 0.1$ atm ($\cdot \cdot$), 1.0 atm ($- -$), 10.0 atm ($- \cdot -$), and 100.0 atm ($-$).

Finally, combining Eqs. (21) and (23) results in

$$\frac{\mu_B \omega}{\gamma p_0} |\hat{p}| = \mu_B \left| \widehat{\nabla \cdot \vec{u}'} \right| = \left| \widehat{p_{\text{eff}} - p} \right|, \quad (24)$$

thus suggesting the dimensionless group

$$\mu_B^* = \frac{\mu_B \omega}{\gamma p_0} = \frac{\mu_B \left| \widehat{\nabla \cdot \vec{u}'} \right|}{|\hat{p}|} = \frac{\left| \widehat{p_{\text{eff}} - p} \right|}{|\hat{p}|}, \quad (25)$$

where μ_B^* is a measure of the relative impact of bulk viscosity on pressure fluctuations.

Traditional attenuation curves, such as Fig. 5, are measured relative to attenuation per meter and tend to belie the effect of bulk viscosity at high frequencies. When measured relative to acoustic wavelength, the bulk viscosity contribution to attenuation can be as large as 1% of pressure amplitude and has a magnitude peak varying

with gas temperature, pressure, and humidity, as shown in Fig. 10.

2. Dimensionless groups

For many fluid problems, dimensionless groups can reduce the number of variables involved, helping to understand the underlying phenomenon and simplifying experiments. However, the proposed bulk viscosity model does not offer a straightforward non-dimensionalization, as the direct application of the Buckingham π theorem to Eqs. (11b), (16) and (19) is limited by constants in the relaxation frequencies (Eq. (14)) and by the saturation vapor pressure.

As a result, for the general air case, neither frequency f nor relative humidity h_r can be part of a useful dimensionless group. Furthermore, temperature T_0 is con-

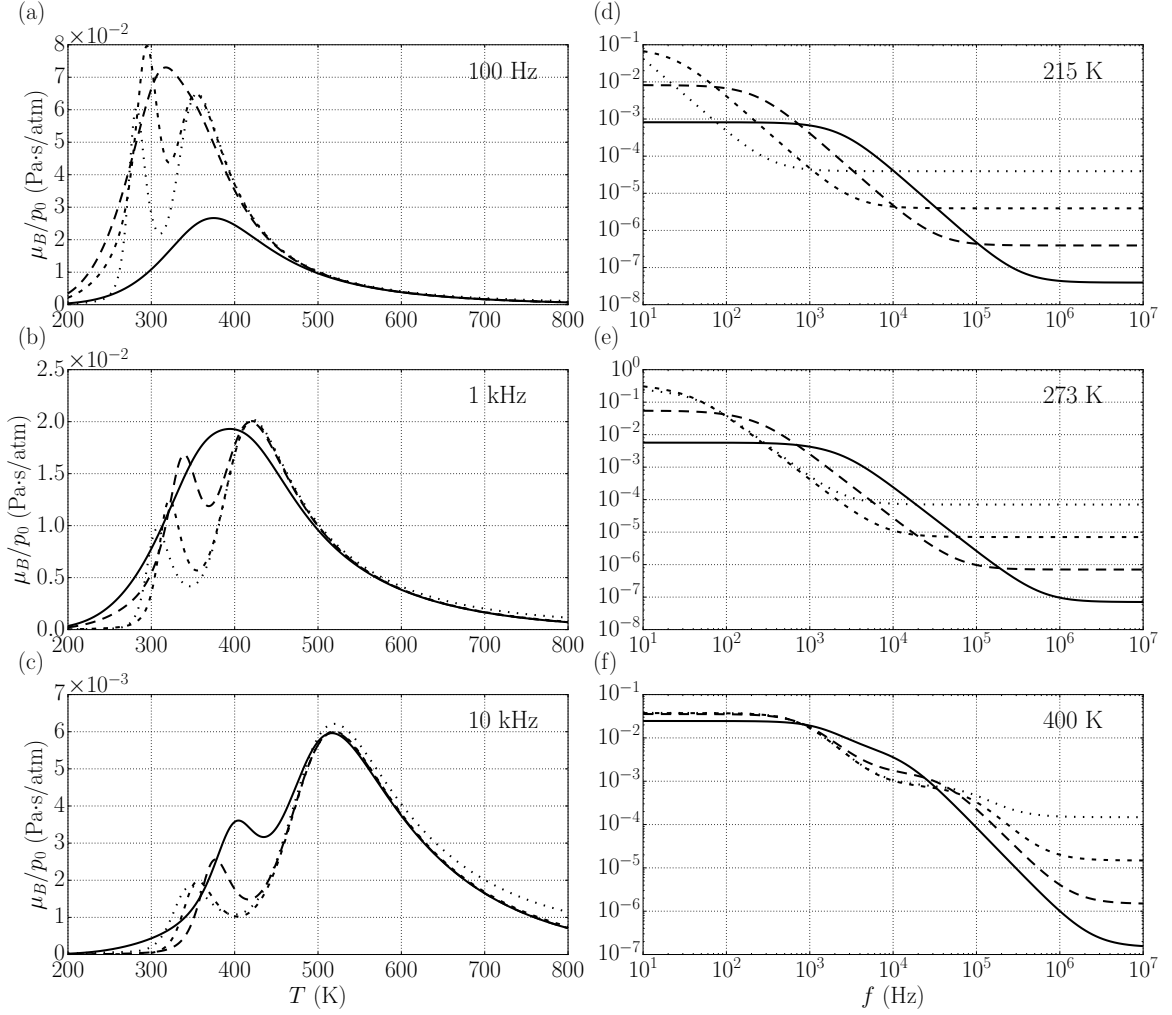


Figure 8. Pressure-normalized bulk viscosity μ_B/p_0 for air at $h_r = 1\%$. Bulk viscosity is plotted against temperature at frequencies of 100 Hz (a), 1 kHz (b), and 10 kHz (c) with pressures $p_0 = 0.1$ atm ($\cdot \cdot$), 1.0 atm ($-\cdot -$), 10.0 atm ($-----$), and 100.0 atm ($—$). Bulk viscosity is plotted against frequency at temperatures of 215.15 K (d), 273.15 K (e), and 400 K (f) with pressures $p_0 = 0.1$ atm ($\cdot \cdot$), 1.0 atm ($-\cdot -$), 10.0 atm ($-----$), and 100.0 atm ($—$).

strained by the triple-point isotherm temperature T_{3p} and pressure p_0 is similarly constrained due to the saturation pressure, p_{sat} , which depends on T_0 .

To find useful scaling parameters, we consider two special cases. In the first case, relative humidity h_r is allowed to vary without bounds. Combining Eqs. (16) and (19) suggests that the dimensionless group μ_B^* remains constant so long as scaling is applied simultaneously to frequency, pressure, and relative humidity,

$$\begin{aligned} \mu_B^* &= \frac{\mu_B \omega}{\gamma p_0} = \text{fn}(f_0, p_0, h_r, T_0) \\ &= \text{fn}(b_1 f_0, b_1 p_0, b_1 h_r, T_0), \end{aligned} \quad (26)$$

for positive scaling parameter b_1 .

The second case considers splitting the dimensionless bulk viscosity into rotational and vibrational relaxational components. The rotational bulk viscosity, as noted before, solely depends on temperature, and the effect as-

sociated with rotational bulk viscosity may be neglected at lower frequencies. Considering instead only the vibrational bulk viscosity, a dimensionless vibrational bulk viscosity

$$\mu_{B,\text{vib}}^* = \frac{\sum_k \mu_{B,\text{vib}}^{(k)} \omega}{\gamma p_0} \quad (27)$$

not only follows the scaling law Eq. (26) but also remains constant if the heat capacity ratio γ is scaled as

$$\begin{aligned} \mu_{B,\text{vib}}^* &= \text{fn}(f_0, p_0, h_r, T_0, \gamma) \\ &= \left(b_2 \frac{(\gamma - 1)^2}{(b_2 \gamma - 1)^2} \right) \text{fn}(b_1 f_0, b_1 p_0, b_1 h_r, T_0, b_2 \gamma), \end{aligned} \quad (28)$$

where both b_1 and b_2 are arbitrary scaling parameters.

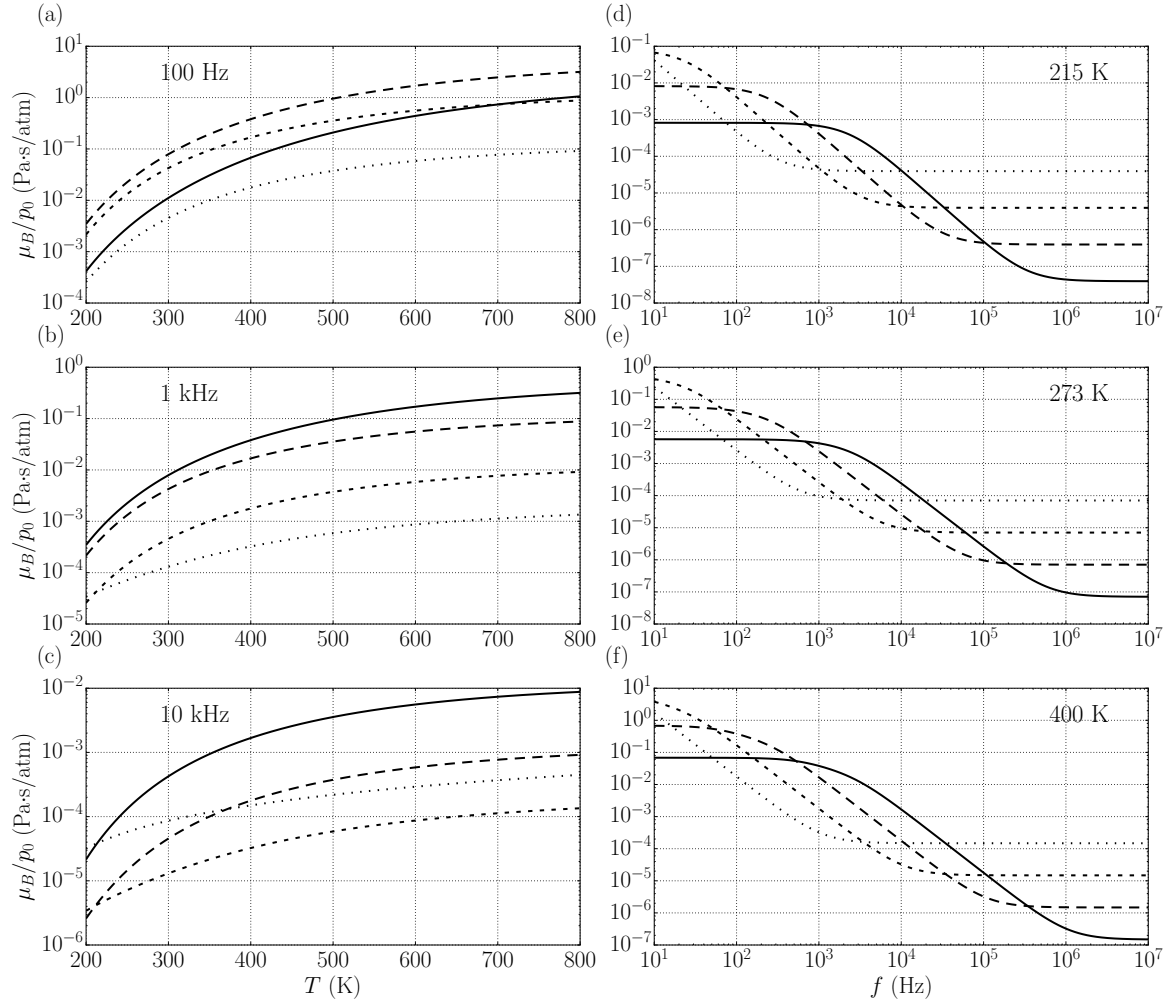


Figure 9. Pressure-normalized bulk viscosity μ_B/p_0 for dry air. Bulk viscosity is plotted against temperature at frequencies of 100 Hz (a), 1 kHz (b), and 10 kHz (c) with pressures $p_0 = 0.1$ atm (\cdots), 1.0 atm ($---$), 10.0 atm ($- \cdot -$), and 100.0 atm ($—$). Bulk viscosity is plotted against frequency at temperatures of 215.15 K (d), 273.15 K (e), and 400 K (f) with pressures $p_0 = 0.1$ atm (\cdots), 1.0 atm ($---$), 10.0 atm ($- \cdot -$), and 100.0 atm ($—$).

For Eq. (28), $\mu_{B,\text{vib}}^* \approx \mu_B^*$ for small f , as shown in Fig. 11. Because γ is related to the degrees of freedom of the fluid in question, it is unlikely that scaling with b_2 can be used without disrupting the general model.

An example of both forms of scaling is shown in Fig. 11. Because the vibrational bulk viscosity has a dominant effect in the low-frequency regime, the scaling of μ_B^* according to Eq. (28) differs by less than 1% for frequencies under 10 kHz.

	A	B	C
f (kHz)	0.5	1	2
p_0 (atm)	0.5	1	2
h_r (ref.)	10%	10%	10%
	▽	□	◇
h_r (similitude)	5%	10%	20%
	▼	■	◆

Table II. Input parameters for self-similar simulations, as used in Fig. 12.

3. Self-similarity of wave attenuation

A dimensionless collapse of the spatial attenuation relationships Eqs. (6) and (10) gives

$$\log P_{amp}^* = \pi [\mu^* + \kappa^* + \mu_B^*] x^* \quad (29)$$

where

$$\begin{aligned} P_{amp}^* &= P_{amp}/P_{amp,0} & x^* &= (x_0 - x)/\lambda \\ \mu^* &= \frac{\omega}{\gamma p_0} \frac{4}{3} \mu & \kappa^* &= \frac{\omega}{\gamma p_0} \frac{(\gamma - 1)^2 \kappa}{\gamma R_{gas}} \end{aligned} \quad (30)$$

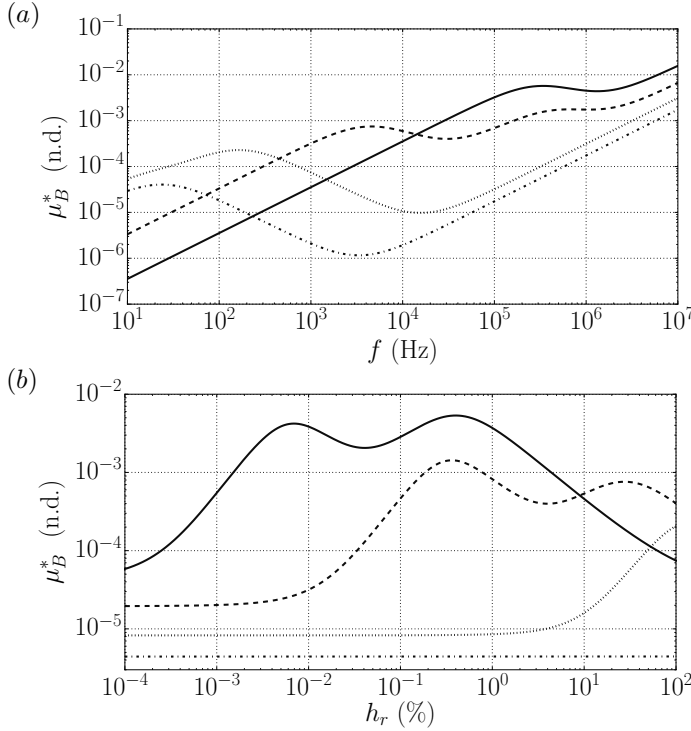


Figure 10. Dimensionless effective bulk viscosity μ_B^* plotted against frequency at $T_0 = 215$ K (·····), 273.15 K (-----), 400 K (- · - ·), and 600 K (—). Results shown for $h_r = 5\%$ and atmospheric pressure (a). Dimensionless effective bulk viscosity μ_B^* plotted against relative humidity, h_r , at $T_0 = 215$ K (·····), 273.15 K (-----), 400 K (- · - ·), and 600 K (—). Results shown for $\omega/2\pi = 25$ kHz and atmospheric pressure (b).

are the chosen normalizations and μ_B^* is as given in Eq. (25).

The similitude scaling in Eq. (26) is tested using the Navier–Stokes simulations, with both imperfect pressure-frequency scaling and pressure-frequency-humidity scaling, as reported in table II. The simulation results are shown in Fig. 12; as expected, the scaling form of Eq. (26) produces self-similar attenuation rates if the simulations account for the effect of humidity in air.

V. CONCLUSION

Bulk viscosity is often neglected in fluid problems, for lack of an established model. We have presented a bulk viscosity model valid for tonal acoustic wave propagation in air, with verification via companion compressible Navier–Stokes simulations and lattice Boltzmann method simulations. The bulk viscosity model captures acoustic attenuation which otherwise is severely underestimated if Stokes’ hypothesis is assumed, and can be a simple addition to both time-domain and frequency-domain solvers. The importance of incorporating bulk viscosity depends on the fluid problem: attenuation related to bulk viscos-

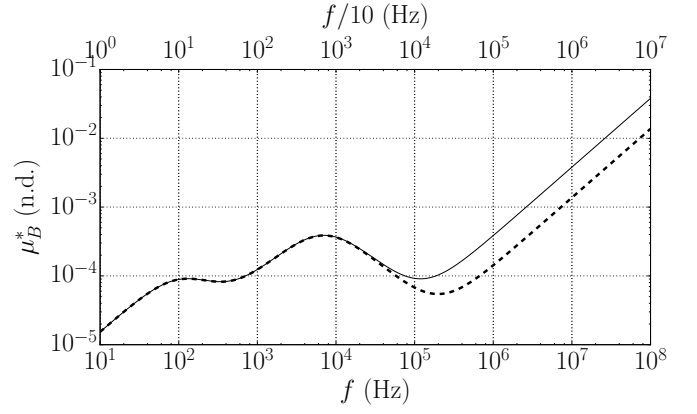


Figure 11. Dimensionless bulk viscosity μ_B^* for air versus frequency at $T_0 = 300$ K for conditions of unscaled f , $p_0 = 1$ atm, $h_r = 10\%$, and $\gamma = 1.4$ (—) and of scaled dimensionless bulk viscosity (see Eq. (28)) for conditions of scaled frequency $f/10$ kHz, $p_0 = 0.1$ atm, $h_r = 1\%$, and $\gamma = 1.66$ (---). This corresponds to scaling parameters of $b_1 = 0.1$ and $b_2 = 1.19$, such that $b_2\gamma = 1.66$. Under conditions of $b_2 = 1$, the plots would be identical.

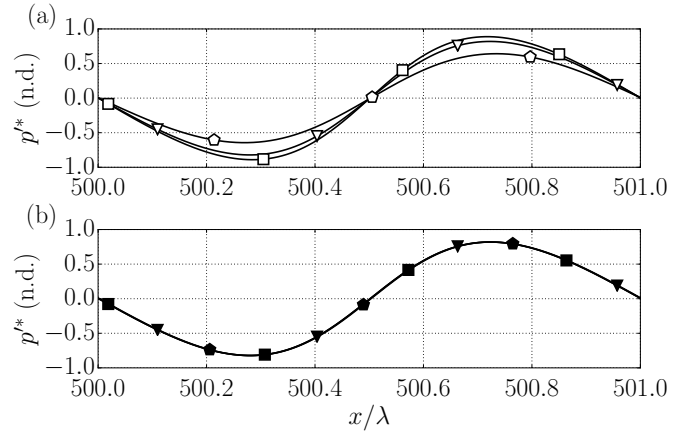


Figure 12. Scaled dimensionless pressure fluctuations $p'^* = p'/P_{amp,0}$ from Navier–Stokes simulations of a freely-traveling wave for acoustic cycle $x/\lambda > 500$ (see Eqs. (29) and (30)) for cases in table II: pressure-frequency similitude scaling (a) and pressure-frequency-humidity scaling (b).

ity is significant at high frequencies when normalized to absolute length scales; at low frequencies, attenuation is significant when normalized by wavelength.

The present model has several limitations: (1) the frequency-dependency of μ_B makes the model unsuitable for broadband time-domain simulations; (2) it cannot capture broadband wave dispersion attributed to μ_B ; and (3) the current modeling framework and the ideal gas assumption can be invalid for dense gases—in such conditions, even monatomic gases can exhibit bulk viscosity effects.³⁷

However, the present model provides several benefits, as it is: (1) algorithmically simple; (2) extensible

to any gaseous mixture provided attenuation measurements and species-specific characteristic molecular vibration temperatures $T_{\text{vib},k}^*$ and relaxation frequencies f_k are known; and (3) applicable to frequency-domain analysis, commonly used in acoustics, and to near-monochromatic time-domain problems.

The relationship between bulk viscosity, pressure, and dilatation is used to construct a bulk viscosity dimensionless group μ_B^* , applicable for both standing- and traveling-wave acoustics problems. Non-dimensional analysis of bulk viscosity suggests that it is a nontrivial function of fluid properties, with limited opportunities to apply similitude. Nevertheless, the bulk viscosity dimensionless group does follow pressure-frequency similitude, with the caveat that relative humidity must be simultaneously varied with pressure and frequency. Because of saturation humidity, such scaling cannot always be possible.

The difference between effective and thermodynamic pressure suggests that the effects of bulk viscosity can be manipulated in situations for which the phasing of pressure and dilatation can be decoupled. Isolating the effects of attenuation due to bulk viscosity from that of shear viscosity can allow for the optimization of geometries where loss is important.

ACKNOWLEDGMENTS

Jeffrey Lin and Carlo Scalo acknowledge the support of the Inventec Stanford Graduate Fellowship and the Precourt Energy Efficiency Center Seed Grant at Stanford University. The authors also acknowledge the generous computational allocation provided to Dr. Scalo on Purdue's latest supercomputing architecture, Rice, and the technical support of Purdue's Rosen Center for Advanced Computing (RCAC). Dr. Scalo acknowledges the support of the Air Force Office of Scientific Research (AFOSR) grant FA9550-16-1-0209 and the very fruitful discussions with Dr. Ivett Leyva (AFOSR) on ultrasonic wave attenuation in hypersonic boundary layers.

Appendix A: Bulk Viscosity Implementation in Time-Domain Simulations

1. Fully compressible Navier–Stokes

The conservation equations for mass, momentum, and energy solved in the fully compressible Navier–Stokes

simulations are, respectively,

$$\frac{\partial}{\partial t}(\rho) + \frac{\partial}{\partial x_j}(\rho u_j) = 0 \quad (\text{A1a})$$

$$\frac{\partial}{\partial t}(\rho u_i) + \frac{\partial}{\partial x_j}(\rho u_i u_j) = -\frac{\partial}{\partial x_i}p + \frac{\partial}{\partial x_j}\tau_{ij} \quad (\text{A1b})$$

$$\frac{\partial}{\partial t}(\rho E) + \frac{\partial}{\partial x_j}[u_j(\rho E + p)] = \frac{\partial}{\partial x_j}(u_i\tau_{ij} - q_j) \quad (\text{A1c})$$

where x_1 , x_2 , and x_3 (equivalently, x , y , and z) are axial and cross-sectional coordinates, u_i are the velocity components in each of those directions, and p , ρ , and E are respectively pressure, density, and total energy per unit mass. The gas is assumed to be ideal, with equation of state $p = \rho R_{\text{gas}} T$ and a constant ratio of specific heats, γ . The gas constant is fixed and calculated as $R_{\text{gas}} = p_{\text{ref}}(T_{\text{ref}}\rho_{\text{ref}})^{-1}$, based on the reference thermodynamic density ρ_{ref} , pressure p_{ref} , and temperature T_{ref} . The viscous and conductive heat fluxes are, respectively,

$$\tau_{ij} = 2\mu \left[S_{ij} + \frac{\mu'}{2\mu} \frac{\partial u_k}{\partial x_k} \delta_{ij} \right] \quad (\text{A2a})$$

$$q_j = -\frac{\mu C_p}{Pr} \frac{\partial T}{\partial x_j} \quad (\text{A2b})$$

where S_{ij} is the strain-rate tensor, given by $S_{ij} = (1/2)(\partial u_j/\partial x_i + \partial u_i/\partial x_j)$; Pr is the Prandtl number; and μ is the dynamic viscosity, given by $\mu = \mu_{\text{ref}}(T/T_{\text{ref}})^{n_\nu}$, where n_ν is the viscosity power-law exponent and μ_{ref} is the reference viscosity. μ' is the second viscosity defined by Eq. (2), $\mu_B \equiv \mu' + \frac{2}{3}\mu$, where μ_B is the effective bulk viscosity value capturing the combined effects of rotational and vibrational molecular relaxation.

Simulations have been carried out with the following gas properties: $\gamma = 1.4$, $\rho_{\text{ref}} = 1.2 \text{ kg m}^{-3}$, $p_{\text{ref}} = 101325 \text{ Pa}$, $T_{\text{ref}} = 300 \text{ K}$, $\mu_{\text{ref}} = 1.98 \times 10^{-5} \text{ kg m}^{-1}\text{s}^{-1}$, $Pr = 0.72$, and $n_\nu = 0.76$, valid for air.³⁸

The governing equations are solved using CharLES^X, a control-volume-based, finite-volume solver for the fully compressible Navier–Stokes equations on unstructured grids, developed as a joint-effort among researchers at Stanford University. CharLES^X employs a three-stage, third-order Runge-Kutta time discretization and a grid-adaptive reconstruction strategy, blending a high-order polynomial interpolation with low-order upwind fluxes.³⁹ The code is parallelized using the Message Passing Interface (MPI) protocol and highly scalable on a large number of processors.⁴⁰

2. Lattice Boltzmann Equations

The LBM solver uses the Bhatnagar-Gross-Krook (BGK) collision model. Variables given in this section will be dimensionless in the LBM solver. The quadra-

ture points selected for each lattice node are

$$\vec{e}_i = \begin{cases} (0, 0) & i = 0 \\ (1, 0), (0, 1), (-1, 0), (0, -1) & i = 1, 2, 3, 4 \\ (1, 1), (-1, 1), (-1, -1), (1, -1) & i = 5, 6, 7, 8, \end{cases} \quad (\text{A3})$$

with corresponding weights of

$$w_i = \begin{cases} 4/9 & i = 0 \\ 1/9 & i = 1, 2, 3, 4 \\ 1/36 & i = 5, 6, 7, 8, \end{cases} \quad (\text{A4})$$

and a streaming and collision update model of

$$\begin{aligned} & f_i(\vec{x}^* + \vec{e}_i, t^* + 1) - f_i(\vec{x}^*, t^*) \\ &= -\frac{1}{\tau^*} [f_i(\vec{x}^*, t^*) - f_i^{eq}(\vec{x}^*, t^*)], \end{aligned} \quad (\text{A5})$$

where f_i is the particle distribution function for each streaming direction, f_i^{eq} is the corresponding equilibrium distribution, and \vec{x}^* , t^* , and τ^* are the non-dimensional grid, time, and relaxation time, respectively. The lattice units are chosen to be $\Delta x^* = \Delta t^* = 1$, such that the non-dimensional lattice speed is $a_0^* = 1/\sqrt{3}$.

The relaxation time τ^* determines the fluid kinematic viscosity,

$$\nu^* = (\tau^* - 1/2) (a_0^*)^2 = \frac{2\tau^* - 1}{6}. \quad (\text{A6})$$

For a channel of defined physical length L and n_x grid points, in order to represent a simulation of physical kinematic viscosity ν_0 and reference density ρ_0 , the conversion from lattice units to physical units is defined as

$$\begin{aligned} x &= C_x x^* & t &= C_t t^* \\ \nu &= C_\nu \nu^* & \rho &= C_\rho \rho^*, \end{aligned} \quad (\text{A7})$$

where

$$\begin{aligned} C_x &= \frac{L}{n_x} & C_t &= \frac{C_x^2}{C_\nu} = \frac{C_x^2 \nu^*}{\nu_0} = \frac{2\tau^* - 1}{6\nu_0} C_x^2 \\ C_\nu &= \frac{C_x^2}{C_t} & C_\rho &= \rho_0. \end{aligned} \quad (\text{A8})$$

a. LBM with MRT

The lattice Boltzmann method in its simplest form assumes equal relaxation times, τ^* , across multiple moments. Multiple relaxation time (MRT) models extend LBM by removing this constraint, allowing different and multiple relaxation times to be used instead. Typically, MRT models replace τ^* as used in the previous section with separate relaxation times for each value. Several of

these relaxation times introduced by MRT correspond to “ghost modes,” which have no basis in kinetic theory, but can enhance stability and indirectly affect fluid flow.⁴¹ Nevertheless, some of these modes have direct physical connections to decoupling bulk and shear viscosity, and the presented model avoids tuning the MRT parameters unphysically. LBM with MRT and the proposed bulk viscosity model (section II) can fully capture acoustic attenuation in air.

For the chosen quadrature points and corresponding weights, the MRT model used is specified by the forward and inverse matrices,

$$M = \begin{pmatrix} 1 & 1 & 1 & 1 & 1 & 1 & 1 & 1 & 1 \\ -4 & -1 & -1 & -1 & -1 & 2 & 2 & 2 & 2 \\ 4 & -2 & -2 & -2 & -2 & 1 & 1 & 1 & 1 \\ 0 & 1 & 0 & -1 & 0 & 1 & -1 & -1 & 1 \\ 0 & -2 & 0 & 2 & 0 & 1 & -1 & -1 & 1 \\ 0 & 0 & 1 & 0 & -1 & 1 & 1 & -1 & -1 \\ 0 & 0 & -2 & 0 & 2 & 1 & 1 & -1 & -1 \\ 0 & 1 & -1 & 1 & -1 & 0 & 0 & 0 & 0 \\ 0 & 0 & 0 & 0 & 0 & 1 & -1 & 1 & -1 \end{pmatrix} \quad (\text{A9a})$$

$$M^{-1} = \frac{1}{36} \begin{pmatrix} 4 & -4 & 4 & 0 & 0 & 0 & 0 & 0 & 0 \\ 4 & -1 & -2 & 6 & -6 & 0 & 0 & 9 & 0 \\ 4 & -1 & -2 & 0 & 0 & 6 & -6 & -9 & 0 \\ 4 & -1 & -2 & -6 & 6 & 0 & 0 & 9 & 0 \\ 4 & -1 & -2 & 0 & 0 & -6 & 6 & -9 & 0 \\ 4 & 2 & 1 & 6 & 3 & 6 & 3 & 0 & 9 \\ 4 & 2 & 1 & -6 & -3 & 6 & 3 & 0 & -9 \\ 4 & 2 & 1 & -6 & -3 & -6 & -3 & 0 & 9 \\ 4 & 2 & 1 & 6 & 3 & -6 & -3 & 0 & -9 \end{pmatrix} \quad (\text{A9b})$$

and the diagonalization of

$$S = \text{diag}(0, s_2, 1.4, 0, s_5, 0, s_7, s_8, s_9), \quad (\text{A10})$$

where it is noted that s_1, s_4, s_6 can be set, without loss of generality, to 0, as mass and momentum are necessarily conserved, $s_5 = s_7$ is required and chosen to be 1.2, and $s_8 = s_9$ is also required and chosen to be $1/\tau^*$.

The bulk viscosity is a tuned parameter and is related to s_2 ; in the MRT model, the shear and bulk kinematic viscosities are, respectively,

$$\nu^* = \frac{\frac{2}{s_8} - 1}{6} = \frac{2\tau^* - 1}{6} \quad (\text{A11})$$

$$\nu_B^* = \frac{\frac{2}{s_2} - 1}{6}. \quad (\text{A12})$$

For implementation, the ratio of bulk viscosity to shear (dynamic) viscosity, μ_B/μ , is used to select s_2 .

REFERENCES

- ¹R. E. Graves and B. M. Argrow, "Bulk Viscosity: Past to Present," *J. Thermophys. Heat Transf.* **13**, 337–342 (1999) .
- ²C. Ener, A. F. Gabrysh, and J. C. Hubbard, "Ultrasonic Velocity, Dispersion, and Absorption in Dry, CO₂-Free Air," *The Journal of the Acoustical Society of America* **24**, 474–477 (1952) .
- ³L. B. Evans, H. E. Bass, and L. C. Sutherland, "Atmospheric Absorption of Sound: Theoretical Predictions," *J. Acoust. Soc. Am.* **51**, 1565–1575 (1972) .
- ⁴A. D. Pierce, *Acoustics: An Introduction to Its Physical Principles and Applications* (Acoustical Society of America, 1989) .
- ⁵H. E. Bass, H.-J. Bauer, and L. B. Evans, "Atmospheric Absorption of Sound: Analytical Expressions," *J. Acoust. Soc. Am.* **52**, 821–825 (1972) .
- ⁶H. E. Bass, L. C. Sutherland, A. J. Zuckerwar, D. T. Blackstock, and D. M. Hester, "Atmospheric absorption of sound: Further developments," *J. Acoust. Soc. Am.* **97**, 680–683 (1995) .
- ⁷H. E. Bass, L. C. Sutherland, A. J. Zuckerwar, D. T. Blackstock, and D. M. Hester, "Erratum: Atmospheric absorption of sound: Further developments [*J. Acoust. Soc. Am.* **97**, 680–683 (1995)]," *J. Acoust. Soc. Am.* **99**, 1259–1259 (1996) .
- ⁸M. S. Cramer, "Numerical estimates for the bulk viscosity of ideal gases," *Phys. Fluids 1994-Present* **24**, 066102 (2012) .
- ⁹M. Roes, M. Hendrix, and J. Duarte, "Contactless energy transfer through air by means of ultrasound," in *IECON 2011 - 37th Annual Conference on IEEE Industrial Electronics Society* (2011) pp. 1238–1243 .
- ¹⁰A. V. Chikitkin, B. V. Rogov, G. A. Tirskey, and S. V. Utyuzhnikov, "Effect of bulk viscosity in supersonic flow past spacecraft," *Applied Numerical Mathematics International Conference Difference Schemes and Applications in Honor of the 90-th Birthday of Professor V. S. Ryaben'kii*, **93**, 47–60 (2015) .
- ¹¹W. L. Nyborg, "Sonically produced heat in a fluid with bulk viscosity and shear viscosity," *J. Acoust. Soc. Am.* **80**, 1133–1139 (1986) .
- ¹²B. C. Eu and Y. G. Ohr, "Generalized hydrodynamics, bulk viscosity, and sound wave absorption and dispersion in dilute rigid molecular gases," *Phys. Fluids 1994-Present* **13**, 744–753 (2001) .
- ¹³A. Claycomb, R. Greendyke, R. Carr, J. Camberos, and R. Branam, "Extending the Validity of the Navier-Stokes Equations by Modifying the Constitutive Relations for Non-Equilibrium," (American Institute of Aeronautics and Astronautics, 2008) .
- ¹⁴A. Claycomb and R. Greendyke, "Extending CFD Modeling to the Transition Regime by Enhanced Thermophysical Modeling," (American Institute of Aeronautics and Astronautics, 2008) .
- ¹⁵R. Wagnild, G. Candler, P. Subbareddy, and H. Johnson, "Vibrational Relaxation Effects on Acoustic Disturbances in a Hypersonic Boundary Layer over a Cone," in *50th AIAA Aerospace Sciences Meeting Including the New Horizons Forum and Aerospace Exposition* (American Institute of Aeronautics and Astronautics, 2012) .
- ¹⁶P. Valentini, T. E. Schwartzentruber, J. D. Bender, I. Nompelis, and G. V. Candler, "Direct molecular simulation of nitrogen dissociation based on an ab initio potential energy surface," *Physics of Fluids* **27**, 086102 (2015) .
- ¹⁷E. M. Salomons, W. J. A. Lohman, and H. Zhou, "Simulation of Sound Waves Using the Lattice Boltzmann Method for Fluid Flow: Benchmark Cases for Outdoor Sound Propagation," *PLoS One* **11** (2016), 10.1371/journal.pone.0147206 .
- ¹⁸E. M. Viggen, "The lattice Boltzmann method: Fundamentals and acoustics," (2014) .
- ¹⁹A. Ern and V. Giovangigli, "Volume Viscosity of Dilute Polyatomic-Gas Mixtures," *Eur. J. Mech. B-Fluids* **14**, 653–669 (1995) .
- ²⁰A. Ern, A. S. Dickinson, and V. Vesovic, "On the behavior of the volume viscosity of atom-molecule mixtures," *J. Chem. Phys.* **121**, 8658–8660 (2004) .
- ²¹A. Ern and V. Giovangigli, "Fast and Accurate Multicomponent Transport Property Evaluation," *Journal of Computational Physics* **120**, 105–116 (1995) .
- ²²H. Medwin, "An Acoustic Streaming Experiment in Gases," *J. Acoust. Soc. Am.* **26**, 332–341 (1954) .
- ²³M. Greenspan, "Rotational Relaxation in Nitrogen, Oxygen, and Air," *J. Acoust. Soc. Am.* **31**, 155–160 (1959) .
- ²⁴W. M. Madigosky, "Density dependence of the bulk viscosity in argon," *J. Chem. Phys.* **46**, 4441–4444 (1967) .
- ²⁵A. S. Dukhin and P. J. Goetz, "Bulk viscosity and compressibility measurement using acoustic spectroscopy," *J. Chem. Phys.* **130**, 124519 (2009) .
- ²⁶T. A. Litovitz and C. M. Davis, "5 - Structural and Shear Relaxation in Liquids," in *Physical Acoustics, Properties of Gases, Liquids, and Solutions* Physical Acoustics, Vol. 2, Part A, edited by W. P. Mason (Academic Press, 1965) pp. 281–349 .
- ²⁷C. W. Chang, G. E. Uhlenbeck, and J. De Boer, "The heat conductivity and viscosity of polyatomic gases," *Stud. Stat. Mech.* **2**, 243–268 (1964) .
- ²⁸G. K. Batchelor, *An Introduction to Fluid Dynamics* (Cambridge University Press, 1973) .
- ²⁹A. A. Sonin, *Equation of Motion for Viscous Fluids* (2001) .
- ³⁰L. D. Landau and E. M. Lifshitz, *Fluid Mechanics* (Elsevier, 2013) .
- ³¹L. Rosenhead, "Introduction. The Second Coefficient of Viscosity: A Brief Review of Fundamentals," *Proceedings of the Royal Society of London. Series A, Mathematical and Physical Sciences* **226**, 1–6 (1954) .
- ³²S. Temkin, *Elements of Acoustics* (Wiley, 1981) .
- ³³G. Emanuel, "Bulk viscosity in the Navier–Stokes equations," *International Journal of Engineering Science* **36**, 1313–1323 (1998) .
- ³⁴P. A. Thompson, *Compressible-Fluid Dynamics* (McGraw-Hill, 1988) .
- ³⁵W. Sutherland, "LII. The viscosity of gases and molecular force," *Lond. Edinb. Dublin Philos. Mag. J. Sci.* **36**, 507–531 (1893) .
- ³⁶J. Latt, *Hydrodynamic Limit of Lattice Boltzmann Equations*, Ph.D. thesis, University of Geneva (2007) .
- ³⁷A. B. Bhatia, *Ultrasonic Absorption: An Introduction to the Theory of Sound Absorption and Dispersion in Gases, Liquids, and Solids* (Courier Corporation, 1985) .
- ³⁸S. De-Yi and W. Bu-Xuan, "Effect of variable thermophysical properties on laminar free convection of gas," *International Journal of Heat and Mass Transfer* **33**, 1387–1395 (1990) .
- ³⁹F. Ham, K. Mattsson, G. Iaccarino, and P. Moin, "Towards Time-Stable and Accurate LES on Unstructured Grids," in *Complex Effects in Large Eddy Simulations*, Lecture Notes in Computational Science and Engineering No. 56, edited by S. C. Kassinos, C. A. Langer, G. Iaccarino, and P. Moin (Springer Berlin Heidelberg, 2007) pp. 235–249 .
- ⁴⁰I. Bermejo-Moreno, J. Bodart, J. Larsson, B. M. Barney, J. W. Nichols, and S. Jones, "Solving the compressible Navier-Stokes equations on up to 1.97 million cores and 4.1 trillion grid points," in *2013 SC - International Conference for High Performance Computing, Networking, Storage and Analysis (SC)* (2013) pp. 1–10 .
- ⁴¹P. Asinari and I. V. Karlin, "Generalized Maxwell state and SHS theorem for computing fluid flows using the lattice Boltzmann method," *Phys. Rev. E* **79**, 036703 (2009) .